Diplofuranoxin, a disubstituted dihydrofuranone, was produced together with sphaeropsidin A and epi-sphaeropsidone by Diplodia subglobosa, an emerging ash (Fraxinus excelsior L.) pathogen in Europe

Diplofuranoxin, a disubstituted dihydrofuranone, was produced together with sphaeropsidin A and epi-sphaeropsidone by *Diplodia subglobosa*, an emerging ash (*Fraxinus excelsior* L.) pathogen in Europe

Marco Masi[a], Roberta Di Lecce[a], Umberto Calice[b], Benedetto Teodoro Linaldeddu[c], Lucia Maddau[d], Stefano Superchi[b], Antonio Evidente[a,*]

[a]Dipartimento di Scienze Chimiche, Università di Napoli Federico II, Complesso Universitario Monte Sant'Angelo, Via Cintia 4, 80126, Napoli, Italy

[b]Dipartimento di Scienze, Università della Basilicata, Viale dell'Ateneo Lucano 10, 85100, Potenza, Italy

[c]Dipartimento Territorio e Sistemi Agro-Forestali, Università degli Studi di Padova, Viale dell'Universit`a 16, Legnaro, 35020, Italy

[d]Dipartimento di Agraria, Sezione di Patologia Vegetale ed Entomologia, Università degli Studi di Sassari, Viale Italia 39, 07100, Sassari, Italy

ABSTRACT

An undescribed disubstituted dihydrofuranone, named diplofuranoxin, was isolated, together with the six well known metabolites sphaeropsidins A and C, *epi*-sphaeropsidone, mellein and *cis*- and *trans*-4-hydroxymelleins, from the fungal species *Diplodia subglobosa*, an emerging pathogen involved in the ash dieback aetiology in Europe. Currently, the disease represents the

main threat to European ash heritage and the wood associated industry. Diplofuranoxin, was characterized essentially by NMR and HRESIMS spectra as (3*Z*)-3-(2,3-dihydroxybutylidene)-5-methyldihydrofuran-2(3*H*)-one. Its relative and absolute configuration was determined by joining NOESY NMR experiments and computational analysis of electronic circular dichroism spectrum. All the metabolites were screened for phytotoxic, antioomycetes and zootoxic activities and only sphaeropsidin A and *epi*-sphaeropsidone were active in two out of three bioassays performed. In addition, sphaeropsidin A completely inhibited mycelium growth of *Phytophthora cambivora*, whereas the inhibition rate of *epi*-sphaeropsidone was less than 50% at the higher concentration used. Both metabolites were inactive in the *Artemia salina* assay. Results obtained in this study have allowed to characterize for the first time the main metabolites produced in vitro by *D. subglobosa* and to increase the knowledge on the metabolic profile of Botryosphaeriaceae for a correct taxonomic classification of the strains belonging to this family.

Keywords:

Fraxinus excelsior, Oleaceae, Canker and dieback, *Diplodia subglobosa*, Botryosphaeriaceae, Invasive pathogens, Phytotoxins, Biological activities

1. Introduction

Fraxinus excelsior L. (Oleaceae), the European ash, is an ecologically and economically important timber species in Europe (Hinsinger et al., 2013). Since the early 90s, severe ash dieback symptoms such as shoot, twig and branch dieback, dark-brown necrotic bark lesions and branch canker have been observed throughout the natural distribution range of the species (Przybył, 2002; Kowalski, 2006; Ogris et al., 2010). The disease was initially associated with the attacks of the exotic and invasive fungus *Hymenoscyphus fraxineus* (T. Kowalski) Baral, Queloz & Hosoya, but recent researches conducted in northern Italy and Slovenia have ascertained that besides *H. fraxineus*, other fungal pathogens belonging to the genus *Diplodia* are involved in the aetiology of the disease (Linaldeddu et al., 2020, 2022). In particular, *Diplodia fraxini* (Fr.: Fr.) Fr., and *Diplodia subglobosa* A.J.L. Phillips, Deidda & Linaldeddu (Botryosphaeriaceae) have been found to be the dominant species associated with branch canker and dieback symptoms, suggesting a primary role of these species in the pathogenic process (Linaldeddu et al., 2020). Despite these new insights into the causes of the disease, many aspects related to the biology of the two *Diplodia* species and to the mechanisms of pathogenesis remain to be clarified. For *H. fraxineus* and *D. fraxini* the capability to produce phytotoxins, some of which characterized by a selective activity towards ash has been ascertained, whereas no information is available for *D. subglobosa* (Cimmino et al., 2017; Masi et al., 2019).

Diplodia subglobosa is a recently described species with a restricted host range and a limited geographical distribution in Europe (Alves et al., 2014). It is phylogenetically related to *Diplodia mutila* (Fr.: Fr.) Fr., *Diplodia africana* Damm & Crous, and *Diplodia olivarum* A.J.L. Phillips, Frisullo & Lazzizera, three polyphagous species able to produce

in vitro a plethora of bioactive compounds including several phytotoxins (Masi et al., 2018; Di Lecce et al., 2021). The interest in phytotoxic metabolites (PMs) produced by *Diplodia* species has increased noticeably over the past decades due to increased incidence of diseases caused by this group of invasive pathogens worldwide (Van Niekerk et al., 2004; Abdollahzadeh, 2015; Cimmino et al., 2016; Smahi et al., 2017; Masi et al., 2021; Reveglia et al., 2021). At the same time, some PMs produced by *Diplodia* species have shown to be versatile compounds with important potential application in the pharmacological sector (Ingels et al., 2017; Roscetto et al., 2020).

Therefore, given the growing expansion of ash dieback in European forests and the still limited information available about the PMs produced by *D. subglobosa*, a study was conducted to isolate, identify, and characterize the main secondary metabolites produced by this emerging pathogen.

2. Results and Discussion

Preliminary experiments were carried to extract *D. subglobosa* culture filtrates using solvent with increasing polarity (n-hexane, chloroform, ethyl ether, and ethyl acetate). Then the phytotoxicity of the corresponding organic extracts was tested and that of ethyl acetate showed the strongest toxicity. The same extract also exhibited the most interesting chromatographic profile, thus ethyl acetate was chosen as solvent to extract the fungal culture filtrates produced in relatively large amount.

The organic extract obtained from the culture filtrates of *D. subglobosa* was purified, as detailed in the Experimental material, obtaining a new trisubstituted dihydrofuranone, named diplofuranoxin (**1**, Fig. 1).

The preliminary ^{1}H and ^{13}C NMR investigation showed that the new specialized metabolite **1** was a disubstituted dihydrofuranone, sharing the molecular formula of

$C_9H_{14}O_4$ as deduced from its HR ESIMS spectrum and consistent with three indices of hydrogen deficiencies.

In addition, its IR (Nakanishi and Solomon, 1977) and UV spectra (Pretsch et al., 2000) showed, in agreement with NMR data, the presence of a conjugated ester carbonyl and hydroxy groups.

The ^{1}H and COSY NMR (Berger and Braun, 2004) (Table 1) showed a broad singlet at δ 6.64, typical of an olefinic proton (H-6), which coupled with the proton (H-7) of the adjacent hydroxylated secondary carbon and the protons (H_2-4) of the adjacent methylene group observed as broad doublet (J = 6.5 Hz) and a complex multiplet at δ 4.18 and 2.43, respectively. H_2-4 coupled with the proton (H-5) of the adjacent secondary oxygenated carbon present as a sextet (J = 6.2 Hz) at δ 4.00, which in turn coupled with the protons (H_3-10) of the geminal methyl group resonating as a doublet (J = 6.2 Hz) at δ 1.23. H-7 also coupled with the proton (H-8) of the adjacent hydroxylated secondary carbon observed as a quintet (J = 6.5 Hz) at δ 3.06 and this in turn with the protons of the terminal methyl group (H_3-9) of the 2,3-dihydroxy-but-1-enyl side chain, observed as a doublet (J = 6.5 Hz) at δ 1.45. The ^{1}H NMR spectrum also showed two broad singlets due to two hydroxyl groups at δ 3.33 and 2.65 (Pretsch et al., 2000).

The ^{13}C and DEPT spectra (Berger and Braun, 2004) (Table 1) showed the presence of one secondary and two tertiary sp^2 carbons, three oxygenated methine, one methylene and two methyl sp^3 carbons. The presence in the ^{13}C NMR spectrum of a carbonyl (C-2) at δ 165.2 which coupled in the HMBC spectrum (Berger and Braun, 2004) (Table 1) with H2-4 and H-6 suggested the presence in **1** of a disubstituted dihydrofuranone ring. The 2,3-dihydroxy-1-butenyl residue is located at C-3 due to the couplings observed in the same spectrum between C-3, at δ 129.2, with H_2-4, H-5, H-7, while those between C4 and C-5 with H3-10 allowed to locate the last methyl group at C-5 (Breitmaier and Voelter, 1987).

The couplings observed in the HSQC spectrum (Berger and Braun, 2004) (Table 1) allowed to assign the chemical shifts to all the protonated carbons and thus the chemical shifts to the all protons and corresponding carbons as reported in Table 1. Thus, diplofuranoxin (**1**) was formulated as 3-(2,3-dihydroxybutylidene)-5-methyldihydrofuran-2(3*H*)-one. This structure was supported from the other couplings observed in the HMBC spectrum (Table 1) and the data of HR ESIMS spectrum. The last spectrum showed the sodiated dimer $[2M + Na]^+$ and the sodiated $[M + Na]^+$ adduct ions at *m/z* 395.1690 and 209.0795. A significant fragmentation ion, generated from the protonated molecular ion $[M + H]^+$ by loss of water was observed at *m/z* 169.

The relative configuration of the double bond of the side chain was assigned by the correlation observed in the NOESY spectrum (Berger and Braun, 2004) (Fig. 2). This latter in addition to the expected correlation between H-8 and H-5 with the protons of the germinal methyl group Me-9 and Me-10 and that between H-6 and H-7, also showed the significant correlation between H-6 and H2-4 wich allowed to assign a *Z*-configuration to the double bond and formulated diplofuranoxin as (3*Z*)-3-(2,3-dihydroxybutylidene)-5-methyldihydrofuran-2(3H)-one (**1**).

To determine the relative and absolute configuration (AC) of **1** a computational analysis (Autschbach, 2012) of its electronic circular dichroism (ECD) spectrum (Superchi et al., 2012, 2018), was undertaken. This approach has proven to be particularly reliable and straightforward for the AC assignment in solution of complex chiral compounds (Vergura et al., 2019) including natural products (Santoro et al., 2020; Vergura et al., 2018). Accordingly, the UV and ECD spectra of **1** were recorded in MeCN in the 190–350 nm range. The ECD spectrum of **1** (Fig. 3) displays three clearly visible and broad Cotton effects (CEs): a negative one at about 262 nm (Δε – 2.22) followed by a positive one at 230 nm (Δε + 3.17) and a more intense negative band at 206 nm (Δε – 5.78). A computational analysis of these chiroptical data by DFT was then carried on. When both

relative and AC are unknown, like in the case of **1**, chiroptical data for any possible stereoisomer should be computed and compared with the experimental data (Masi et al., 2021; Johnson et al., 2018). In this case, the presence of three stereocenters implies the existence of eight possible stereoisomer (four pairs of enantiomers) for each double bond configuration. It follows, that the computational analysis must be performed on the (5*S**,7*S**,8*S**), (5*S**,7*S**,8*R**), (5*S**,7*R**,8*R**), and (5*S**,7*R**,8*S**) diastereomers for both *Z* and *E*. Since enantiomeric diastereomers have mirror image ECD spectra, for each compound it is sufficient to predict the chiroptical properties for only one enantiomer of the possible diastereomers. Although NMR NOESY analysis (*vide supra*) indicated a *Z* double bond geometry of **1** this assignment was verified by carrying out computational treatment also on the *E* diastereomer. Therefore, conformational analysis on the four arbitrarily chosen stereoisomers (5*S*,7*S*,8*S*)-**1a**, (5*S*,7*S*,8*R*)-**1b**, (5*S*,7*R*,8*R*)-**1c**, and (5*S*,7*R*,8*S*)-**1d** for both *Z* and *E* configuration (Fig. 4), was carried out at DFT/B3LYP/6-31G(d)/IEFPCM(MeCN) level of theory taking into account solvation effects by the polarized continuum solvation model (IEFPCM) (Tomasi et al., 2005). The structure and relative population of main conformers for each stereoisomer was thus obtained. Then, ECD and UV spectra for each found conformer were computed at TDDFT/CAM-B3LYP/aug-cc-pvdz/IEFPCM(MeCN) level and Boltzmann averaged over conformers population.

In Figs. S1 and S2 in Supplementary Information, S.I. the computed spectra of each stereoisomer and of the corresponding enantiomer are compared with the experimental spectra for **1**. As inferred from Fig. S1 and Fig. S2, the best agreement with experimental is provided by computed ECD spectra of ***Z*-1a** and ***Z*-1b** stereoisomers. In fact, the computed spectra of *E* diastereomers ***E*-1a-d** appears opposite in sign to the experimental in correspondence to the two long wavelength bands at 230 and 262 nm, while spectra of their enantiomers **ent-*E*-1a-d** better fit those two bands, but are opposite

in sign to the high energy Cotton effect at 206 nm (Fig. S2). The same behaviour is observed by computed ECD spectra of ***Z*-1c,d** and those of their enantiomers ***Z*-1c,d**. While the formers agree with the high energy band, the latters agree with the other two bands. Only ***Z*-1a** and ***Z*-1b** spectra fit in sign, wavelength and intensity with all the three main Cotton effects of the experimental (Fig. S1). This analysis allows to confirm the previous assignment of *Z* configuration of the double bond as well as the (5*S*) absolute configuration of the lactone stereocenter, but is not sufficient to allow a sure choice between the (5*S*,7*S*,8*S*)-***Z*-1a** and (5*S*,7*S*,8*R*)-***Z*-1b** stereoisomers which both fit experimental, even if with some small spectral differences. Therefore, spectral computational analysis of both these stereoisomers was carried out at a higher computational level. Accordingly, previously found conformers of (3*Z*,5*S*,7*S*,8*S*)-***Z*-1a** and (3*Z*,5*S*,7*S*,8*R*)-***Z*-1b** were further optimized at DFT/B3LYP/6–311++G(d,p)/IEFPCM(MeCN) level and their UV and ECD spectra computed at TDDFT/CAMB3LYP/aug-cc-pvtz/IEFPCM(MeCN) level, providing, after Boltzmann averaging, spectra reported in Fig. 3. Spectral comparison with experimental now clearly indicates a better agreement of (3*Z*,5*S*,7*S*,8*S*)-***Z*-1a** than (3*Z*,5*S*,7*S*,8*R*)-***Z*-1b**, allowing to assign (3*Z*,5*S*,7*S*,8*S*) relative and absolute configuration to **1**.

The dihydrosapinofuranones are well known as phytotoxic metabolites produced by plant pathogenic fungi (Masi et al., 2018). Among them the most similar to **1** are pinofuranoxins A and B, two phytotoxins produced by *Diplodia sapinea* (Fr.) Fuckel a worldwide conifer pathogen. They differed from **1** for the stereochemistry and the functionalities of the 1-butenyl side chain attached to C-6 (Masi et al., 2021).

The well known phytotoxins sphaeropsidins A and C, epi-sphaeropsidone, mellein and *cis*- and *trans*-4-hydroxymelleins (**2**–**7**, Fig. 1), isolated for the first time from *D. subglobosa*, were identified by comparing their physic (specific optical rotation, see S.I.) and spectroscopic data (^{1}H NMR and ESI MS, see: S.I.) with those reported in literature.

In particular, for **2** with the data reported by Evidente et al. (1996), for **3** by Evidente et al. (1997), for **4** by Evidente et al. (1998) for **5**, **6** and **7** by Cabras et al. (2006).

All metabolites (**1**–**7**) obtained in this study were screened for phytotoxic, antioomycetes and zootoxic activities.

Phytotoxicity was determined using the leaf puncture bioassay and evaluated on *Phaseolus vulgaris* L. leaves at concentration of 0.4 mg/mL. Sphaeropsidin A (**2**) and *epi*-sphaeropsidone (**4**) were active, to different extents, in this bioassay. Specifically, sphaeropsidin A (**2**) caused necrotic lesions on the plant species tested with a lesion size of 24.9 ± 1.6 mm^2 *epi*-Sphaeropsidone (**4**) caused lesions with a lesion size of 15.8 ± 3.9 mm^2. None of the other compounds caused any visible symptoms in this bioassay.

The antioomycete activity of the isolated compounds was evaluated towards *Phytophthora cambivora* (Petri) Buisman, the causal agent of "ink disease" on chestnut, at concentration of 0.2 and 0.02 mg/plug. Metalaxyl-M was used as positive control. Among the metabolites assayed, sphaeropsidin A (**2**) inhibited completely the mycelial growth of *P. cambivora* at both concentrations. *epi*-Sphaeropsidone (**4**) inhibited only partially the *P. cambivora* growth (37% at concentration of 0.2 mg/plug). No colony growth inhibition was observed with the other compounds at the higher concentration used.

Additionally, the compounds **1**–**7** were screened for lethality in the brine shrimp (*Artemia salina* L.) larvae bioassay, which is widely used for toxicology and ecotoxicology studies. All metabolites were tested at concentration of 50 μg/mL, resulting all inactive.

3. Conclusions

The manuscript reports the structure and AC assignment of a novel trisubstituted dihydrofuranone from *D. subglobosa* named diplofuranoxin (**1**). The findings obtained in this study have allowed us to characterize for the first time the metabolic profile of *D.*

subglobosa and expand the scientific knowledge about PMs produced by Botryosphaeriaceae. The results confirm the broad spectrum of activities of the sphaeropsidin A and, to a different extent, of the *epi*-sphaeropsidone. In particular, the activity in controlling *P. cambivora* is of particular application interest given the broad spectrum of host plants and the virulence of this pathogen for which there are no effective management strategies. Some compounds produced by *D. subglobosa* are also produced by other *Diplodia* spp. and the sphaeropsidin A confirmed to be the main phytotoxic metabolite produced by this group of fungal pathogens. Finally, the spectrum of activities of the new metabolite (**1**) deserves more detailed investigations and in particular it is necessary to evaluate a potential phytotoxic activity towards ash.

4. Experimental material

4.1. General experimental procedures

Optical rotations were measured in a MeOH solution on a Jasco P-1010 digital polarimeter; IR spectra were recorded as a glassy film on a Perkin-Elmer Spectrum One Fourier Transform Infrared (FTIR) spectrometer. UV spectra were recorded on a JASCO V-530 spectrophotometer in CH_3CN solution, while ECD spectra were recorded at room temperature on a JASCO J815 spectropolarimeter, by using 0.5 mm cells and concentration of 6.5×10^{-3} M for **1** in CH_3CN solution; ^{1}H and ^{13}C NMR spectra were recorded at 400 and 100 MHz, respectively, in $CDCl_3$ on a Bruker spectrometer. The same solvent was used as an internal standard. Carbon multiplicities were determined by DEPT spectra (Berger and Braun, 2004). DEPT, COSY-45, HSQC, HMBC, and NOESY experiments (Berger and Braun, 2004) were performed using Bruker microprograms. HRESI and ESI mass spectra were performed as previously described (Masi et al., 2021). Analytical and preparative TLC were performed on silica gel plates (Kieselgel 60, F_{254}, 0.25 and 0.5 mm respectively) or on reverse phase (KC_{18} F_{254}, 0.20 mm) plates and the

compounds were visualized by exposure to UV light and/or iodine vapors and/or by spraying first with 10% H_2SO_4 in MeOH, and then with 5% phosphomolybdic acid in EtOH, followed by heating at 110 ◦C for 10 min. CC: silica gel (Merck, Kieselgel 60, 0.063–0.200 mm).

4.2. Fungal strain

The *Diplodia subglobosa* A.J.L. Phillips, Deidda & Linaldeddu (Botryosphaeriaceae) strain used in this study was isolated from a symptomatic branch of European ash (*Fraxinus excelsior* L., Oleaceae), collected in Veneto region (north-eastern, Italy) (Linaldeddu et al., 2020). The strain was identified on the basis of morphological characters and analysis of internal transcribed spacer (ITS) rDNA. Fungal DNA extraction, PCR amplification reactions, and DNA sequencing were carried out as reported by Linaldeddu et al. (2020). The sequence of the ITS region has been deposited in GenBank (accession number: ON505148). Pure cultures were maintained on PDA slants under oil at 10 ◦C in the dark in the culture collection of the Dipartimento Territorio e Sistemi Agro-forestali, Universit`a degli Studi di Padova, Italy, as FB68.

4.3. Production, extraction and purification of the metabolites

The fungus was grown on liquid medium (Czapek amended with 2% yeast extract; pH 5.7). The cultures were filtered through filter paper (Whatman N.1) and the filtrates (22 L) exhaustively extracted with EtOAc yielding an oily brown residue (8.1 g). This latter was purified by silica gel column chromatography (CC), eluting with CHCl3-*iso*-PrOH (9:1, v/v) and nine homogeneous (F1–F9) fractions were collected. The residue (600.2 mg) of the second fraction (F2) was purified by CC, eluted with petroleum ether/acetone (8:2, v/v), yielding six homogeneous fractions (F2.1-F2.6). The fraction F2.2 resulted to be an homogeneous compound, which was identified as mellein (**5**, 15.4 mg, R_f

0.73). The residue (70.1 mg) of F2.4 was purified by preparative TLC developed twice, using petroleum ether–acetone (8:2) as solvent system yielding two white solid identified as (3*R*,4*R*)-(–)-4-hydroxymellein (**6**) (23.4 mg, R_f 0.25) and (3*R*,4*S*)-(–)-4-hydroxymellein (**7**) (21.0 mg, R_f 0.32). The residue (876.5 mg) of the third fraction of the first column (F3) was purified by CC, eluted with CH_2Cl_2–MeOH (95:5, v/v), yielding seven fractions (F3.1-F3.7). The residue (268.9 mg) of F3.3 was crystallized using EtOAc-n-hexane (1:3, v/v) at room temperature yielding white crystals identified as sphaeropsidin A (**2**, 232.8 mg, R_f 0.61). The residue (40.6 mg) of F3.4 was further purified by preparative TLC eluted with CH_2Cl_2-*iso*-PrOH (95:5, v/v) yelding an amorphous solid identified as sphaeropsidin C (**3**, 31.8 mg, R_f 0.37). The residue (78.1 mg) of F5 was further purified by preparative through TLC CH_2Cl_2–MeOH (9:1, v/v) yielding and amorphous oil identified as *epi*-sphaeropsidone (**4**, 13.8 mg, R_f 0.59). The residue (120 mg) of F6 was further purified by TLC, eluted with EtOAc-*n*-hexane (9:1, v/v), yielding as an amorphous solid diplofuranoxin (**1**, 6.7 mg, R_f 0.34).

4.3.1 Diplofuranoxin (1)

Amorphous solid, IR ν_{max} 3377, 1702, 1062 cm^{-1}; UV λ_{max} (log ε) 198 (0.90) nm; ^1H and ^{13}C NMR see Table 1; HRESI MS (+): *m/z* 395.1690 $[2M + Na]^+$ and 209.0795 $[M + Na]^+$ (calcd for $C_9H_{14}NaO_4$, 209.0790).

4.4. Computational details

Preliminary conformational analysis was performed by Spartan02 package (Spartan 02, 2002) employing MMFF94s molecular mechanics (MM) force field with Monte Carlo searching and fixing arbitrarily the following absolute configurations for *E* and *Z* diastereomers **1a-d** of **1**: (*Z*,5*S*,7*S*,8*S*)-***Z*-1a**, (*Z*,5*S*,7*S*,8*R*)-***Z*-1b**, (*Z*,5*S*,7*R*,8*R*)-***Z*-1c**, and (*Z*,5*S*,7*R*,8*S*)-***Z*-1d** for *Z* configuration and (*E*,5*S*,7*S*,8*S*)-***E*-1a**, (*E*,5*S*,7*S*,8*R*)-***E*-1b**,

(*E*,5*S*,7*R*,8*R*)-***E*-1c**, and (*E*,5*S*,7*R*,8*S*)-***E*-1d** configuration for *E* configuration. All possible conformers were searched, considering the degrees of freedom of the system, retaining only the structures within an energy range of 30 kcal/mol with respect to the most stable one. The minimum energy conformers found by MM were further fully optimized by using the Density Functional Theory (DFT) approach at DFT/B3LYP/6-31G(d)/IEFPCM(MeCN) level of theory by Gaussian09 package (Frisch et al., 2009) and taking into account the solvent effect of CH_3CN by IEFPCM implicit model (Tomasi et al., 2005). All conformers are real minima, no imaginary vibrational frequencies have been found and the free energy values have been calculated and used to get the Boltzmann population of conformers at 298.15 K (Belviso et al., 2019). The found geometries were employed as input geometries for calculation of UV and ECD spectra at the TDDFT/CAM-B3LYP/aug-cc-pvdz/IEFPCM(MeCN) level. Further optimization of the **Z-1a** and **Z-1b** diastereoisomers was carried out at DFT/B3LYP/6–311++G(d,p)/IEFPCM(MeCN) level and their UV and ECD spectra computed at TDDFT/CAM-B3LYP/aug-cc-pvtz/IEFPCM(MeCN) level. The theoretical UV and ECD spectra were obtained as average over the conformers Boltzmann populations. The ECD spectra were obtained by the Spec Dis v1.51 package (Bruhn et al., 2013) from calculated excitation energies and rotational strengths, as a sum of Gaussian functions centered at the wavelength of each transition, with a parameter σ (width of the band at ½ height) of 0.4 eV.

4.5. Leaf puncture assay

Phaseolus vulgaris L. leaves were used for this assay. Each compound, dissolved in DMSO, was tested at 0.4 mg/mL. The assay was performed as previously reported (Andolfi et al., 2014). DMSO in distilled water (4%) was used as control. Each treatment was repeated two times. Leaves were observed daily and scored for symptoms after 5

days. The effect of the toxins on the leaves was observed up to 10 days. Lesions were estimated using APS Assess 2.0 software following the tutorials in the user's manual. The lesion size was expressed in mm^2.

4.6. Antifungal assays

All compounds (1–7) were also preliminarily tested on *Phytophthora cambivora*. The sensitivity of this species to these compounds was evaluated on CA (carrot agar medium) as inhibition of the mycelial radial growth. The assay was performed as previously reported (Masi et al., 2021). Each metabolite was tested at 0.2 and 0.02 mg/plug. DMSO was used as negative control and Metalaxyl-M (mefenoxam; p.a. 43.88%; Syngenta), a synthetic fungicide to which the oomycetes are sensitive, was used as positive control. Each treatment consisted of three replicates and the experiment was repeated twice.

4.7. Artemia salina bioassay

All compounds were also assayed on brine shrimp larvae (*Artemia salina* L.). The assay was performed in cell culture plates with 24 cells as previously described (Andolfi et al., 2014). The metabolites were tested at 50 µg/mL. DMSO was used as negative control. Tests were performed in quadruplicate. The percentage of larval mortality was determined after 36 h incubation at 27 °C in the dark.

Declaration of competing interest

The authors declare that they have no known competing financial interests or personal relationships that could have appeared to influence the work reported in this paper.

Acknowledgment

This study was also partially supported by the "Fondo di Ateneo per la ricerca 2020", an internal funding provided by the University of Sassari and by the project "Ruolo di *Diplodia fraxini* e *Diplodia subglobosa* nell'eziologia del deperimento del frassino in Italia", grant number DOR2021428/20 UNIPD. Financial support by Project PON RI 2014–2020 BIOFEEDSTOCK (grant number ARS01_00985) financed by MIUR is also gratefully acknowledged. Prof. Antonio Evidente is associated to Istituto di Chimica Biomolecolare del CNR, Pozzuoli, Italy. Prof. Antonio Evidente and Dr. Marco Masi are associated to BAT Center – Interuniversity Center for Studies on Bioinspired Agro-Environmental Technology, University of Napoli "Federico II", Portici (NA), Italy.

Appendix A. Supplementary data

Supplementary data to this article can be found online at https://doi.org/10.1016/j.phytochem.2022.113302.

References

Abdollahzadeh, J., 2015. *Diplodia bulgarica*, as a new pathogen and potential threat to the apple industryin Iran. Phytopathol. Mediterr. 54, 128–132 https://doi.org/10.14601/Phytopathol_Mediterr-14686.

Alves, A., Linaldeddu, B.T., Deidda, A., Scanu, B., Phillips, A.J.L., 2014. The complex of *Diplodia* species associated with *Fraxinus* and some other woody hosts in Italy and Portugal. Fungal Divers. 67, 143–156. https://doi.org/10.1007/s13225-014-0282-9.

Andolfi, A., Maddau, L., Basso, S., Linaldeddu, B.T., Cimmino, A., Scanu, B., Deidda, A., Tuzi, A., Evidente, A., 2014. Diplopimarane, a 20-nor-ent-pimarane produced by the oak pathogen *Diplodia quercivora*. J. Nat. Prod. 77, 2352–2360. https://doi.org/10.1021/np500258r.

Autschbach, J., 2012. Ab initio electronic circular dichroism and optical rotatory dispersion: from organic molecules to transition metal complexes. In: Berova, N., Polavarapu, P.L., Nakanishi, K., Woody, R.W. (Eds.), Comprehensive Chiroptical Spectroscopy, vol. 1. John Wiley & Sons, Inc., Hoboken, NJ, pp. 593–642. https://doi.org/10.1002/9781118120187.ch21 (Chapter 21).

Belviso, S., Santoro, E., Penconi, M., Righetto, S., Tessore, F., 2019. Thioethyl porphyrazines: attractive chromophores for second-order nonlinear optics and DSSCs. J. Phys. Chem. C 123, 13074–13082. https://doi.org/10.1021/acs.jpcc.9b02654.

Berger, S., Braun, S., 2004. 200 and More Basic NMR Experiments: a Practical Course, first ed. Wiley-VCH, Weinheim, ISBN 978-3-527-31067-8.

Breitmaier, E., Voelter, W., 1987. Carbon-13 NMR Spectroscopy. VCH, Weinheim, ISBN 3-527-26466-3.

Bruhn, T., Schauml¨offel, A., Hemberger, Y., Bringmann, G., 2013. SpecDis: quantifying the comparison of calculated and experimental electronic circular dichroism spectra. Chirality 25, 243–249. https://doi.org/10.1002/chir.22138.

Cabras, A., Mannoni, M.A., Serra, S., Andolfi, A., Fiore, M., Evidente, A., 2006. Occurrence, isolation and biological activity of phytotoxic metabolites produced *in vitro* by *Sphaeropsis sapinea*, pathogenic fungus of *Pinus radiata*. Eur. J. Plant Pathol. 115, 187–193. https://doi.org/10.1007/s10658-006-9006-7.

Cimmino, A., Maddau, L., Masi, M., Evidente, M., Linaldeddu, B.T., Evidente, A., 2016. Further secondary metabolites produced by *Diplodia corticola*, a fungal pathogen involved in cork oak decline. Tetrahedron 72, 6788–6793. https://doi.org/10.1016/j.tet.2016.09.008.

Cimmino, A., Maddau, L., Masi, M., Linaldeddu, B.T., Pescitelli, G., Evidente, A., 2017. Fraxitoxin, a new isochromanone isolated from *Diplodia fraxini*. Chem. Biodivers. 14, e1700325 https://doi.org/10.1002/cbdv.201700325.

Di Lecce, R., Masi, M., Linaldeddu, B.T., Piscitelli, G., Maddau, L., Evidente, A., 2021. Bioactive secondary metabolites produced by the emerging pathogen *Diplodia olivarum*. Phytopathol. Mediterr. 60, 129–138. https://doi.org/10.36253/phyto-12170.

Evidente, A., Sparapano, L., Motta, A., Giordano, F., Fierro, O., Frisullo, S., 1996. A phytotoxic pimarane diterpene of *Sphaeropsis sapinea* f. sp. *cupressi*, the pathogen of a canker disease of cypress. Phytochemistry 42, 1541–1546. https://doi.org/10.1016/0031-9422(96)00206-3.

Evidente, A., Sparapano, L., Fierro, O., Bruno, G., Giordano, F., Motta, A., 1997. Sphaeropsidins B and C, phytotoxic pimarane diterpenes from *Sphaeropsis sapinea*

f. sp. *cupressi* and *Diplodia mutila*. Phytochemistry 45, 705–713. https://doi.org/10.1016/S0031-9422(97)00006-X.

Evidente, A., Sparapano, L., Fierro, O., Bruno, G., Giordano, F., Motta, A., 1998. Sphaeropsidone and episphaeropsidone, phytotoxic dimedone methylethers produced by *Sphaeropsis sapinea* f. sp. *cupressi* grown in liquid culture. Phytochemistry 48, 1139–1143. https://doi.org/10.1016/S0031-9422(97)00897-2.

Frisch, M.J., et al., 2009. GAUSSIAN 09, Revision A.02. Gaussian, Inc., Wallingford, CT.

Hinsinger, D.D., Basak, J., Gaudeul, M., Cruaud, C., Bertolino, P., Frascaria-Lacoste, N., Bousquet, J., 2013. The phylogeny and biogeographic history of ashes (Fraxinus, Oleaceae) highlight the roles of migration and vicariance in the diversification of temperate trees. PLoS One 8, e80431. https://doi.org/10.1371/journal.pone.0080431.

Ingels, A., Dinhof, C., Garg, A.D., Maddau, L., Masi, M., Evidente, A., Berger, W., Dejaegher, B., Mathieu, V., 2017. Computed determination of the *in vitro* optimal chemocombinations of sphaeropsidin A with chemotherapeutic agents to combat melanomas. Cancer Chemother. Pharmacol. 79, 971–983. https://doi.org/10.1007/s00280-017-3293-x.

Johnson, J.L., Raghavan, V., Cimmino, A., Moeini, A., Petrovic, A.G., Santoro, E., Superchi, S., Berova, N., Evidente, A., Polavarapu, P.L., 2018. Absolute configurations of chiral molecules with multiple stereogenic centers without prior

knowledge of the relative configurations: a case study of inuloxin C. Chirality 30, 1206–1214. https://doi.org/10.1002/chir.23013.

Kowalski, T., 2006. *Chalara fraxinea* sp. nov. associated with dieback of ash (*Fraxinus excelsior*) in Poland. For. Pathol. 36, 264–270. https://doi.org/10.1111/j.1439-0329.2006.00453.x.

Linaldeddu, B.T., Bottecchia, F., Bregant, C., Maddau, L., Montecchio, L., 2020. *Diplodia fraxini* and *Diplodia subglobosa*: the main species associated with cankers and dieback of *Fraxinus excelsior* in North-Eastern Italy. Forests 11, 883. https://doi.org/10.3390/f11080883.

Linaldeddu, B.T., Bregant, C., Montecchio, L., Brglez, A., Piˇskur, B., Ogris, N., 2022. First report of *Diplodia fraxini* and *Diplodia subglobosa* causing canker and dieback of Fraxinus excelsior in Slovenia. Plant Dis. 106, 26. https://doi.org/10.1094/PDIS-06-21-1204-SC.

Masi, M., Di Lecce, R., Marsico, G., Linaldeddu, B.T., Maddau, L., Superchi, S., Evidente, A., 2021. Pinofuranoxins A and B, bioactive trisubstituted furanones produced by the invasive pathogen *Diplodia sapinea*. J. Nat. Prod. 84, 2600–2605. https://doi.org/10.1021/acs.jnatprod.1c00365.

Masi, M., Di Lecce, R., Tuzi, A., Linaldeddu, B.T., Montecchio, L., Maddau, L., Evidente, A., 2019. Hyfraxinic acid, a phytotoxic tetrasubstituted octanoic acid, produced by the ash (*Fraxinus excelsior* L.) pathogen *Hymenoscyphus fraxineus* together with

viridiol and some of its analogues. J. Agric. Food Chem. 67, 13617–13623. https://doi.org/10.1021/acs.jafc.9b06055.

Masi, M., Maddau, L., Linaldeddu, B.T., Scanu, B., Evidente, A., Cimmino, A., 2018. Bioactive metabolites from pathogenic and endophytic fungi of forest trees. Curr. Med. Chem. 25, 208–252. https://doi.org/10.2174/0929867324666170314145159.

Nakanishi, K., Solomon, P.H., 1977. Infrared Absorption Spectroscopy, second ed. Holden Day, Oakland, ISBN 0-816-26251-9, pp. 17–44.

Ogris, N., Hauptman, T., Jurc, D., Floreancig, V., Marsich, F., Montecchio, L., 2010. First report of Chalara fraxinea on common ash in Italy. Plant Dis. 94, 133. https://doi. org/10.1094/PDIS-94-1-0133A.

Pretsch, E., Bühlmann, P., Affolter, C., 2000. Structure Determination of Organic Compounds – Tables of Spectral Data, third ed. Springer-Verlag, Berlin, ISBN 3-540-67815-8, pp. 161–243.

Przybył, K., 2002. Fungi associated with necrotic apical parts of *Fraxinus excelsior* shoots. For. Pathol. 32, 387–394. https://doi.org/10.1046/j.1439-0329.2002.00301.x.

Reveglia, P., Billones-Baaijens, R., Millera Niem, J., Masi, M., Cimmino, A., Evidente, A., Savocchia, S., 2021. Production of phytotoxic metabolites by Botryosphaeriaceae in naturally infected and artificially inoculated grapevines. Plants 10, 802. https://doi.org/10.3390/plants10040802.

Roscetto, E., Masi, M., Esposito, M., Di Lecce, R., Delicato, A., Maddau, L., Calabro, V., Evidente, A., Catania, M.R., 2020. Anti-biofilm activity of the fungal phytotoxin sphaeropsidin A against clinical isolates of antibiotic-resistant bacteria. Toxins 12, 444. https://doi.org/10.3390/toxins12070444.

Santoro, E., Vergura, S., Scafato, P., Belviso, S., Masi, M., Evidente, A., Superchi, S., 2020. Absolute configuration assignment to chiral natural products by biphenyl chiroptical probes: the case of the phytotoxins colletochlorin A and agropyrenol. J. Nat. Prod. 83, 1061–1068. https://doi.org/10.1021/np300770s.

Smahi, H., Belhoucine-Guezouli, L., Berraf-Tebbal, A., Chouih, S., Arkam, M., Franceschini, A., Linaldeddu, B.T., Phillips, A.J.L., 2017. Molecular characterization and pathogenicity of *Diplodia corticola* and other Botryosphaeriaceae species associated with canker and dieback of *Quercus suber* in Algeria. Mycosphere 8, 1261–1272. https://doi.org/10.5943/mycosphere/8/2/10.

SPARTAN ’02; Wavefunction Inc.: Irvine, CA; http://www.wavefunction.com.

Superchi, S., Rosini, C., Mazzeo, G., Giorgio, E., 2012. Determination of molecular absolute configuration: guidelines for selecting a suitable chiroptical approach. In: Berova, N., Polavarapu, P.L., Nakanishi, K., Woody, R.W. (Eds.), Comprehensive Chiroptical Spectroscopy, vol. 2. John Wiley & Sons, Inc., Hoboken, NJ, pp. 421–447. https://doi.org/10.1002/9781118120392.ch12.

Superchi, S., Scafato, P., Gorecki, M., Pescitelli, G., 2018. Absolute configuration determination by quantum mechanical calculation of chiroptical spectra: basics and

applications to fungal metabolites. Curr. Med. Chem. 25, 287–320. https://doi.org/10.2174/0929867324666170310112009.

Tomasi, J., Mennucci, B., Cammi, R., 2005. Quantum mechanical continuum solvation models. Chem. Rev. 105, 2999–3094. https://doi.org/10.1021/cr9904009.

Van Niekerk, J.M., Crous, P.W., Fourie, P.H., Hallen, F., 2004. DNA phylogeny, morphology and pathogenicity of Botryosphaeria species on grapevines. Mycologia 96, 781–798. https://doi.org/10.1080/15572536.2005.11832926.

Vergura, S., Santoro, E., Masi, M., Evidente, A., Scafato, P., Superchi, S., Mazzeo, G., Longhi, G., Abbate, S., 2018. Absolute configuration assignment to anticancer Amaryllidaceae alkaloid jonquailine. Fitoterapia 129, 78–84. https://doi.org/10.1016/j.fitote.2018.06.013.

Vergura, S., Scafato, P., Belviso, S., Superchi, S., 2019. Absolute configuration assignment from optical rotation data by means of biphenyl chiroptical probes. Chem. Eur J. 25, 5682–5690. https://doi.org/10.1002/chem.201806435.

Legends for Figures

Fig. 1. Structure and assigned absolute configuration (see text) of diplofuranoxin (**1**) and that of the already known phytotoxic metabolites sphaeropsidins A and C (**2** and **3**), *epi*-sphaeropsidone (**4**) mellein and *cis*- and *trans*-4- hydroxy melleins (**5**–**7**).

Fig. 2. The NOE correlations observed in the NOESY spectrum of **1**.

Fig. 3. Comparison between experimental ECD spectrum (solid red line) of **1** with calculated ECD spectra [TDDFT/CAM-B3LYP/aug-cc-pvtz/IEFPCM(MeCN)] for (*Z*) stereoisomers *Z*-**1a,b** (blue dashed line) and their enantiomers **ent**-*Z*-**1a,b** (green dashed line). Panel (a) (3*Z*,5*S*,7*S*,8*S*)-*Z*-**1a**; panel (b) (3*Z*,5*S*,7*S*,8*R*)-*Z*-**1b**. Conformers population computed at DFT/B3LYP/6–311++G(d,p)/IEFPCM(MeCN) level. For a better spectral comparison computed spectra are shifted of +25 nm. (For interpretation of the references to colour in this figure legend, the reader is referred to the Web version of this article.)

Fig. 4. Stereoisomers of **1** taken into account in ECD computations.

Fig. 1.

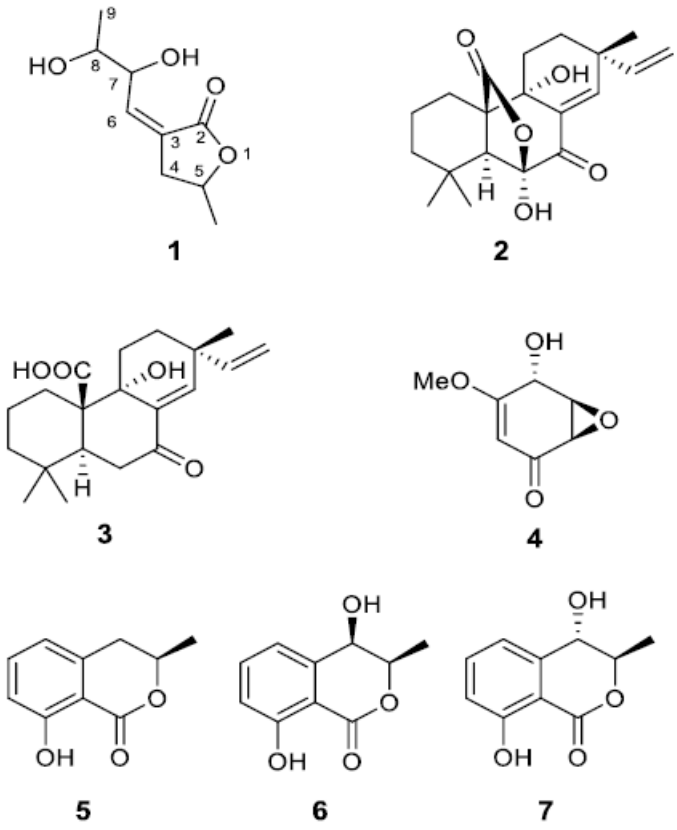

Fig. 2.

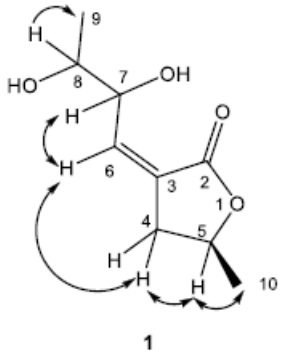

Fig. 3.

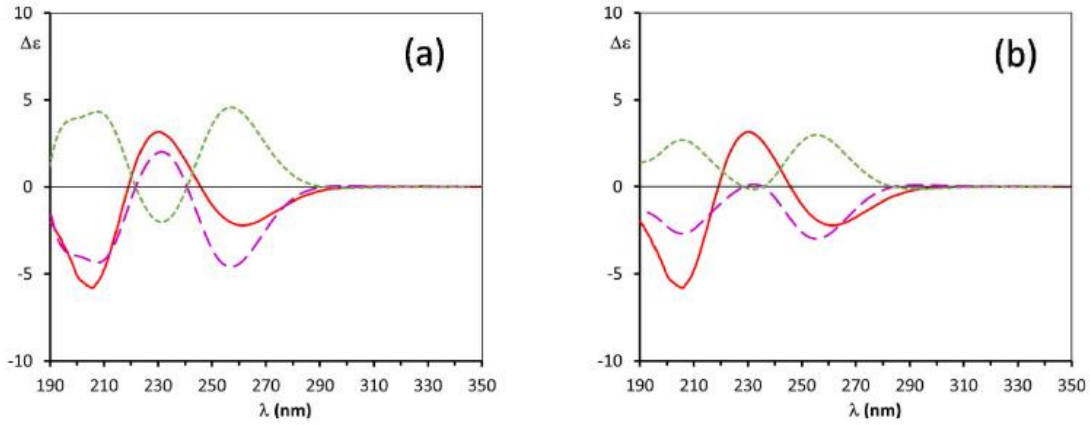
(a)
(b)
Δε
λ (nm)
10
5
0
-5
-10
190
210
230
250
270
290
310
330
350

Fig. 4.

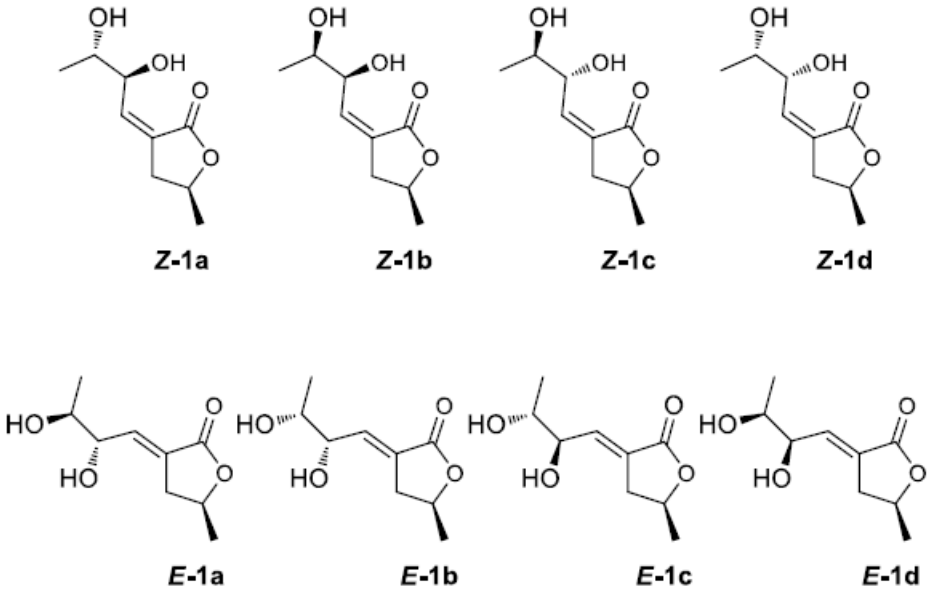
OH
HO
O
Z-1a
Z-1b
Z-1c
Z-1d
E-1a
E-1b
E-1c
E-1d

Table 1
^{1}H and ^{13}C NMR data of diplofuranoxin (**1**)[a,b].

No.	δ_C[c]	δ_H (*J* in Hz)	HMBC
2	165.2 s		H_2-4, H-6
3	129.2 d		H_2-4, H-5, H-7
4	39.7 t	2.43 (2H) m	H_3-10
5	66.9 d	4.00 (1H) sext (6.2)	H_2-4, H_3-10
6	144.3 d	6.64 (1H) br s	H_2-4, H-8
7	67.6 d	4.18 (1H) br d (6.5)	H-8, H_3-9
8	79.4 d	3.06 (1H) quint (6.5)	H-6, H_3-9
9	18.1 q	1.45 (3H) d (6.5)	
10	23.3 q	1.23 (3H) d (6.2)	H_2-4
HO-7		3.33 br s[d]	
OH-8		2.65 br s[d]	

[a] 2D 1H, 1H (COSY) and ^{13}C, ^{1}H (HSQC) NMR experiments confirmed the correlations of all the protons and the corresponding carbons.
[b] Coupling constants (*J*) are given in parenthesis.
[c] Multiplicities were assigned with DEPT.
[d] These two signals can be exchanged.